Journal of Applied Mechanics and Technical Physics, Vol. 47, No. 3, pp. 330–339, 2006

LARGE EDDY SIMULATION IN A FULLY DEVELOPED TURBULENT FLOW IN A CHANNEL AND COMPARISON OF SUBGRID EDDY VISCOSITY MODELS

K. N. Volkov

UDC 532.529:536.24

The accuracy and computational efficiency are compared for a number of models of subgrid eddy viscosity (Smagorinsky model, renormalization group model, and dynamic and one-parameter models). Space-filtered Navier–Stokes equations are solved numerically by the control-volume approach on a nonuniform grid with the use of high-resolution schemes in time and space. The numerical data are compared with the results of a physical experiment and direct numerical simulation.

Key words: *turbulence, large eddy simulation, subgrid viscosity, internal flows.*

Introduction. Despite the intense development of computational technologies and achievements in construction of numerical methods and development of appropriate software, numerical simulation of turbulence remains one of the most complicated and important problems in fluid dynamics. In contrast to a laminar flow whose computation has already become a routine procedure, reliable prediction of turbulent flow parameters is more art than rigorous science for numerous reasons (three-dimensional character of the flow; stochastic nature and wide spatial and temporal spectrum of scales).

The initial pre-requisite for mathematical modeling of turbulence is the assumption that the Navier–Stokes equations are acceptable for interpreting turbulent flows and for predicting instantaneous characteristics of these flows [1, 2].

Numerous methods of numerical simulation of turbulent flows include direct numerical simulation (DNS), large eddy simulation (LES), and solving Reynolds-averaged Navier–Stokes (RANS) equations. There are also intermediate (hybrid) approaches that combine these or those features of DNS, RANS, and LES, in particular, detached eddy simulation (DES) [3].

Direct numerical simulation implies solving the full Navier–Stokes equations, which allows obtaining instantaneous characteristics and resolving all scales of a turbulent flow, if numerical and other types of errors can be avoided. The resultant statistics is used to test turbulence models, to develop methods of turbulent flow control, and to study the laminar–turbulent transition. As the capabilities of measurement equipment are limited, DNS is considered as a source of experimental data (e.g., such parameters of the flow as pressure fluctuations, vorticity, and rate of dissipation of turbulent energy).

Obstacles in using DNS are high requirements to difference schemes, satisfaction of initial and boundary conditions, and limited computational resources [1, 2]. Steps of integration in time and space have the order of Kolmogorov's scales of time and length and decrease with increasing Reynolds number [2]. Obtaining a statistically steady flow pattern requires tens and hundreds of hours of processor time. The use of unstructured grids also contributes to consumption of computer memory and processor time. Because of requirements listed above, it is difficult to implement computations that involve DNS (except for low Reynolds numbers and simple flow geometry).

University of Surrey, Guildford GU2 7XH, UK; dsci@mail.ru. Translated from Prikladnaya Mekhanika i Tekhnicheskaya Fizika, Vol. 47, No. 3, pp. 31–42, May–June, 2006. Original article submitted January 18, 2005; revision submitted July 6, 2005.

 0021-8944/06/4703-0330

Solving RANS equations requires much lower computational resources and is successfully used in practice. The issues of closure are solved at different levels of complexity [1]. Turbulence models are classified in terms of the number of equations introduced in addition to the Reynolds equations. An increase in the number of equations requires additional semi-empirical information to be involved, which spoils model universality. Available models of turbulence do not possess acceptable universality and, therefore, cannot be used to solve a wide range of applied problems.

The absence of a universal turbulence model suitable for computing all or, at least, most turbulent flows shifted the focus in turbulence research. Improved capabilities of computational engineering simulated the search for and application of approaches that are more rigorous and universal than RANS.

Large eddy simulation is a compromise between DNS and RANS. LES implies solving space-filtered Navier–Stokes equations. Large eddies, being under a direct action of boundary conditions and carrying the maximum Reynolds stresses, are calculated. Small vortices have a more universal structure and are modeled by subgrid scale (SGS) models constructed on the concept of eddy viscosity or other rational approximations of transport processes. Subgrid models are normally characterized by significant diffusion and dissipation, which allows one to overcome computational problems caused by presentation of small vortices on a chosen grid and to stabilize numerical computations [1, 4].

As LES does not allow direct computations of small vortices, the difference grids and time steps are much greater (approximately by an order of magnitude) than Kolmogorov's scales of length and time. Higher Reynolds numbers than in the DNS method can be reached with a fixed computational memory. The main LES problem, however, is determining derivatives for resolving the finest scales [4, 5].

A large number of subgrid models, filters, boundary conditions, and finite-difference schemes have been tested in numerous computations [5–7]. Nevertheless, neither the optimal choice of the subgrid model is clear nor the choice, if made, is justified [1]. There are no universal near-wall functions reducing the number of nodes in the vicinity of the wall; hence, it is difficult to use LES for computing flows with small separation regions and transition points [3, 7], e.g., for computing the flow around an airfoil at incidence [6]. Yet, LES is a promising direction in the development of methods for computing turbulent flows and seems to be a serious alternative to DNS and RANS.

The accuracy and computational efficiency for a number of models of subgrid eddy viscosity [Smagorinsky model, renormalization group (RNG) model, and dynamic and one-parameter models] are compared in the present work as applied to computing a fully developed turbulent channel flow. The numerical data are compared with the results of a physical experiment and direct numerical simulation.

1. Governing Equations. In the Cartesian coordinate system (x, y, z), the unsteady flow of a viscous compressible gas is described by the following equation written for space-filtered quantities:

$$\frac{\partial \boldsymbol{Q}}{\partial t} + \frac{\partial \boldsymbol{F}}{\partial x} + \frac{\partial \boldsymbol{G}}{\partial y} + \frac{\partial \boldsymbol{H}}{\partial z} = 0. \tag{1}$$

Equation (1) is supplemented by the equation of state for a perfect gas:

$$p = (\gamma - 1)\rho[e - (u^2 + v^2 + w^2)/2].$$

The vector of conservative variables $\boldsymbol{Q}$ and the flux vectors $\boldsymbol{F}$, $\boldsymbol{G}$, and $\boldsymbol{H}$ have the following form:

$$\boldsymbol{Q} = \begin{pmatrix} \rho \\ \rho u \\ \rho v \\ \rho w \\ \rho e \end{pmatrix},$$

$$\boldsymbol{F} = \begin{pmatrix} \rho u \\ \rho uu + p - \tau_{xx} \\ \rho uv - \tau_{xy} \\ \rho uw - \tau_{xz} \\ (\rho e + p)u - u\tau_{xx} - v\tau_{xy} - w\tau_{xz} + q_x \end{pmatrix},$$

$$\boldsymbol{G} = \begin{pmatrix} \rho v \\ \rho v u - \tau_{yx} \\ \rho v v + p - \tau_{yy} \\ \rho v w - \tau_{yz} \\ (\rho e + p) v - u\tau_{yx} - v\tau_{yy} - w\tau_{yz} + q_y \end{pmatrix},$$

$$\boldsymbol{H} = \begin{pmatrix} \rho w \\ \rho w u - \tau_{zx} \\ \rho w v - \tau_{zy} \\ \rho w w + p - \tau_{zz} \\ (\rho e + p) w - u\tau_{zx} - v\tau_{zy} - w\tau_{zz} + q_z \end{pmatrix}.$$

The components of the viscous stress tensor and the components of the heat-flux vector are found from the relations

$$\tau_{ij} = \mu_e \Big(\frac{\partial v_i}{\partial x_j} + \frac{\partial v_j}{\partial x_i} - \frac{2}{3} \frac{\partial v_k}{\partial x_k} \delta_{ij} \Big), \qquad q_i = -\chi_e \frac{\partial T}{\partial x_i},$$

where t is the time, ρ is the density, u, v, and w are the velocity components in the coordinate directions x, y, and z, respectively, p is the pressure, e is the total energy of a mass unit, T is the temperature, γ is the ratio of specific heats, τ is the shear stress, and δ_{ij} is the Kronecker symbol.

Equation (1) is suitable for both laminar and turbulent flows. In modeling turbulent flows, the molecular transport coefficients are replaced by their effective values. Effective viscosity μ_e is calculated as the sum of molecular viscosity μ and subgrid turbulent viscosity μ_{sgs}, whereas effective thermal conductivity χ_e is expressed via viscosity and the Prandtl number as

$$\mu_e = \mu + \mu_{\text{sgs}}, \qquad \chi_e = c_p(\mu/\text{Pr} + \mu_{\text{sgs}}/\text{Pr}_{\text{sgs}}),$$

where c_p is the specific heat at constant pressure, $\text{Pr} = 0.72$, and $\text{Pr}_{\text{sgs}} = 0.9$.

2. Subgrid Scale Models. To close the space-filtered Navier–Stokes equations (1), we use the hypothesis of eddy viscosity.

2.1. *Smagorinsky Model.* In the Smagorinsky model [8], subgrid viscosity is calculated as

$$\mu_{\text{sgs}} = \rho(C_{\text{S}}\Delta)^2 |S|, \tag{2}$$

where

$$|S| = (2S_{ij}S_{ij})^{1/2}, \qquad S_{ij} = \frac{1}{2}\Big(\frac{\partial v_i}{\partial x_j} + \frac{\partial v_j}{\partial x_i} \Big).$$

It is usually assumed that $C_{\text{S}} \approx 0.1$. To take into account the influence of the wall on the mixing length, Eq. (2) is supplemented by the Van Driest damping function

$$f_\mu = 1 - \exp\left[-(y^+/25)^3\right],$$

where $y^+ = \rho u_\tau y/\mu$, $u_\tau = (\tau_{\text{w}}/\rho)^{1/2}$, and τ_{w} is the friction stress on the wall.

2.2. RNG *Model.* In the renormalization group theory, subgrid viscosity is calculated by solving the nonlinear equation [9]

$$\mu_{\text{sgs}} = \mu[1 + H(X - C)]^{1/3}, \qquad X = 2A\Big(\frac{\Delta}{2\pi} \Big)^4 \frac{\mu_{\text{sgs}}}{\mu^3} |S|^2. \tag{3}$$

Here $H(X)$ is the Heaviside function, $A = 0.12$, and $C = 75$. For $X \gg C$, Eq. (3) reduces to the Smagorinsky formula (2), and

$$C_{\text{S}} = (2\pi)^2 \sqrt{A/2} = 0.0062.$$

2.3. *Dynamic Model.* The dynamic model [10] involves information contained in resolvable scales to estimate the Smagorinsky parameter.

The formulation of the dynamic model starts from the Smagorinsky eddy viscosity approximation. The so-called probe or test filter is introduced, the transmission band of this filter $\hat{\Delta}$ being greater than the width of the initial (grid) filter Δ used for filtering the Navier–Stokes equations (it is normally assumed that $\hat{\Delta} = 2\Delta$). Density

is considered as a function of time only, but not as a function of spatial coordinates. The value of the parameter $C_{\rm S}$ is assumed to be unchanged during secondary filtration.

We introduce a second-order tensor L_{ij} (the so-called Leonard stress tensor) whose components are equal to the difference between the components of subgrid stress tensors T_{ij} and $\tilde{\tau}_{ij}$:

$$L^*_{ij} = L_{ij} - (1/3)\delta_{ij}L_{kk} = (T_{ij} - \hat{\tau}_{ij})/\rho = \widehat{\tilde{v}_i\tilde{v}_j} - \hat{\tilde{v}}_i\hat{\tilde{v}}_j = -2C_{\rm S}\hat{\Delta}^2 M_{ij}.$$

Here $M_{ij} = (\hat{\Delta}/\Delta)^2|\hat{\tilde{S}}|\hat{\tilde{S}}_{ij} - |\tilde{S}|\tilde{S}_{ij}$. The quantity L_{ij} is the contribution of vortices whose sizes vary from Δ to $\hat{\Delta}$ to the Reynolds stress.

The value of the parameter $C_{\rm S}\Delta$ is chosen by minimizing the error given by the quantity

$$Q = E_{ij}E_{ij},$$

where

$$E_{ij} = L^*_{ij} - T_{ij} + \hat{\tau}_{ij} = L^*_{ij} + 2C_E M_{ij}, \qquad C_E = (C_{\rm S}\Delta)^2.$$

Using the least squares technique and averaging over the volume, we can write

$$\frac{\partial E^2}{\partial C_E} = \frac{\partial\langle E_{ij}E_{ij}\rangle}{\partial C_E} = 2\Big\langle E_{ij}\,\frac{\partial E_{ij}}{\partial C_E}\Big\rangle = 0.$$

Taking into account that $\partial E_{ij}/\partial C_E = 2M_{ij}$, we obtain

$$C_E = -(1/2)\langle L_{ij}M_{ij}\rangle/\langle M_{kl}M_{kl}\rangle.$$

The value of the parameter $C_{\rm S}$ calculated by the dynamic procedure significantly oscillates in space and time. A specific difficulty resulting from these oscillations is a possibly negative value of eddy viscosity ($C_{\rm S} < 0$). This feature means energy transfer from subgrid vortices to resolvable scales [9]. In principle, such a process may occur in an unsteady flow, but it usually leads to computational instability [5]. To prevent this, $C_{\rm S}$ is averaged over uniform directions, which damps high-frequency harmonics. At the $(n+1)$th time step, we use the lower relaxation, which suppresses high-frequency oscillations

$$C_{\rm S}^{n+1} = (1-\omega)C_{\rm S}^n + \omega C_{\rm S}^*,$$

where ω is the coefficient of lower relaxation ($\omega \approx 10^{-3}$).

2.4. *Differential Model.* Eddy viscosity can be expressed in terms of the subgrid turbulent kinetic energy

$$\mu_{\rm sgs} = \rho(C_{\rm S}\Delta)k_{\rm sgs}^{1/2}.$$

The subgrid turbulent kinetic energy is found by soling the equation

$$\frac{\partial\rho k_{\rm sgs}}{\partial t} + \frac{\partial\rho v_j k_{\rm sgs}}{\partial x_j} = \frac{\partial}{\partial x_j}\Big[\Big(\mu + \frac{\mu_{\rm sgs}}{\sigma_k}\Big)\frac{\partial k_{\rm sgs}}{\partial x_j}\Big] - c_\varepsilon\,\frac{k_{\rm sgs}^{3/2}}{\Delta}. \tag{4}$$

It is assumed in Eq. (4) that $\sigma_k = 0.7$ and $c_\varepsilon = 0.845$.

3. Width of the Filter. The computed results depend on the filter width Δ, which enters the filtration operator and is related to the difference-grid step:

$$\Delta = V^{1/3} = (\Delta x\,\Delta y\,\Delta z)^{1/3}$$

(V is the cell volume and Δx, Δy, and Δz are the grid steps in the coordinate directions x, y, and z, respectively).

The grid step in the boundary layer in the normal-to-wall direction Δy is replaced by $\hat{\Delta}y$, and the filter width is found from the relation

$$\Delta = (\Delta x\,\hat{\Delta}y\,\Delta z)^{1/3},$$

where $\hat{\Delta}y = \Delta y$ in the vicinity of the wall and $\hat{\Delta}y = \bar{\Delta}y$ far from the wall (a smooth transition between the indicated limiting values is used for intermediate values of y). The quantity $\bar{\Delta}y$ is the mean value of Δy in the near-wall region, and $\hat{\Delta}y$ is calculated by the formula

$$\hat{\Delta}y = [(1/\Delta y)^\alpha + (1/\bar{\Delta}y)^\alpha]^{-1/\alpha},$$

where $\alpha = 3$.

A smaller width of the filter allows reproduction of a wider frequency range of fluctuations of flow parameters, whereas an increase in Δ facilitates smoothing of the solution (LES transforms to DNS as $\Delta \to 0$).

4. Initial and Boundary Conditions. Velocity, pressure, and temperature distributions are set as the initial conditions at the time $t = 0$.

Uniform velocity, density, and pressure profiles ($u = u_0$, $\rho = \rho_0$, and $p = p_0$) with superimposed random perturbations of a given amplitude (white noise) are prescribed in the initial cross section of the channel. No-slip boundary conditions are set for velocity components on the wall, as well as the wall temperature $T_{\rm w}$.

Modeling of unsteady subsonic flows faces the problem of setting the boundary conditions for the exhausting gas flow containing intense vortex structures. Possible non-physical effects of generation and reflection of acoustic waves at the exit boundary distort the real pattern of the flow. All sought functions at the exit of the computational domain are subjected to the convective transfer conditions (non-reflecting boundary conditions)

$$\frac{\partial f}{\partial t} + U\,\frac{\partial f}{\partial n} = 0,$$

where U is the velocity independent of the exit-boundary position and chosen from the condition of conservation of mass.

5. Numerical Method. Nonlinear interactions with resolvable scales and corresponding wavenumbers produce waves with wavenumbers higher than the critical one, which can be interpreted numerically [4] (compatibility). If no special precautions are taken, this effect can be interpreted as fictitious energy transfer to low wavenumbers [4] (negative turbulent viscosity).

Discretization of Eq. (1) is performed by the control-volume approach on a nonuniform grid [11]. To move the solution in time and present the spatial derivatives on the finest scales, we use high-resolution finite-difference schemes. In contrast to the mean velocity, the accuracy of predicting velocity fluctuations strongly depends on the order of the difference scheme [5].

Equation (1) is written in the form

$$\frac{dQ^n_{i,j,k}}{dt} + L(Q^n_{i,j,k}) = 0,$$

where

$$L(Q^n_{i,j,k}) = \frac{F^n_{i+1/2,j,k} - F^n_{i-1/2,j,k}}{\Delta x_{i,j,k}} + \frac{G^n_{i,j+1/2,k} - G^n_{i,j-1/2,k}}{\Delta y_{i,j,k}} + \frac{H^n_{i,j,k+1/2} - H^n_{i,j,k-1/2}}{\Delta z_{i,j,k}}.$$

The three-step Runge–Kutta method is used for discretization in time [12]:

$$Q^{(1)}_{i,j,k} = Q^{(n)}_{i,j,k} + \Delta t\, L(Q^{(n)}_{i,j,k}),$$

$$Q^{(2)}_{i,j,k} = \frac{3}{4}\,Q^{(n)}_{i,j,k} + \frac{1}{4}\,[Q^{(1)}_{i,j,k} + \Delta t L(Q^{(1)}_{i,j,k})], \qquad Q^{(n+1)}_{i,j,k} = \frac{1}{3}\,Q^{(n)}_{i,j,k} + \frac{2}{3}\,[Q^{(2)}_{i,j,k} + \Delta t L(Q^{(2)}_{i,j,k})].$$

The stability region has the form of a circumference of radius $r_{\rm c}$ (a difference scheme is stable if $\Delta t < r_{\rm c}$). The stability region in the complex plane has the form of a circle

$$x + iy = r\exp(i\theta).$$

The radius of the stability region is found from the relation

$$r_{\rm c} = \min_{\theta} r(\theta) \qquad \text{at} \quad \pi/2 \leqslant \theta \leqslant 3\pi/2.$$

In particular, $r_{\rm c} = 1.25$ for the three-step Runge–Kutta method. The Runge–Kutta method is advantageous because it ensures that the difference scheme is positive (if the solution at the time t^n is positive, it remains positive at the time t^{n+1} as well).

The flux vector is divided into the inviscid and viscous components. The use of centered difference schemes for discretization of convective components at high Reynolds numbers leads to computational instability and unphysical oscillations of the solution. Discretization of inviscid fluxes is performed with the use of the method of piecewise-parabolic reconstruction and the Chakravarthy–Osher scheme [13], whereas discretization of viscous fluxes involves the use of second-order centered finite-difference schemes. The method of discretization of diffusion fluxes affects the technical aspect of implementation of the approach. A lower order of discretization of viscous terms is interpreted

as a small inaccuracy in presenting viscous forces, which is admissible if turbulent viscosity is calculated by an approximate model.

The inviscid flux is found from the relation

$$F(Q_L, Q_R) = [F(Q_L) + F(Q_R) - |A|(Q_R - Q_L)]/2.$$

The subscripts L and R refer to cells on the left and on the right of the control-volume face.

The matrix A is presented as $A = R|\Lambda|L$, where Λ is the diagonal matrix composed of Jacobian eigenvalues; R and L are the matrices composed of the right and left eigen vectors of this Jacobian.

The Chakravarthy–Osher scheme implies a piecewise-parabolic distribution of the sought variables within the control volume [13]. The intermediate step deals with determining the auxiliary variables

$$\alpha^i_{1,m+1/2} = l^i_{m+1/2}(Q_m - Q_{m-1}),$$

$$\alpha^i_{2,m+1/2} = l^i_{m+1/2}(Q_{m+1} - Q_m), \qquad \alpha^i_{3,m+1/2} = l^i_{m+1/2}(Q_{m+2} - Q_{m+1}).$$

Here $l = \{l_1, l_2, \ldots\}$ is the set of left eigenvectors; the superscript i refers to the ith eigenvalue and ith eigen vector; the subscripts 1, 2, and 3 are used for numeration.

The family of schemes satisfying the total variation diminishing (TVD) condition has the form

$$F_{m+1/2} = H_{m+1/2} + \sum_i \Big(\frac{1+\varkappa}{4}\,\tilde\alpha^i_{2,m+1/2} + \frac{1-\varkappa}{4}\,\tilde{\tilde\alpha}^i_{2,m+1/2}\Big)\lambda^{i+}_{m+1/2}\,r^i_{m+1/2}$$

$$- \sum_i \Big(\frac{1+\varkappa}{4}\,\tilde{\tilde\alpha}^i_{2,m+1/2} + \frac{1-\varkappa}{4}\,\tilde\alpha^i_{3,m+1/2}\Big)\lambda^{i+}_{m+1/2}\,r^i_{m+1/2},$$

where $\lambda = \{\lambda_1, \lambda_2, \ldots\}$ and $r = \{r_1, r_2, \ldots\}$ are the set of eigenvalues and the set of right eigen vectors. The first term in the right side determines the flux by a first-order scheme

$$H_{m+1/2} = \frac{1}{2}\,[F(Q_{m+1/2}) + F(Q_m)] - \frac{1}{2}\sum_i (\lambda^{i+}_{m+1/2} - \lambda^{i-}_{m+1/2})\alpha^i_{2,m+1/2} r^i_{m+1/2}.$$

Here

$$\tilde{\tilde\alpha}^i_{1,m+1/2} = \operatorname{minmod}\{\alpha^i_{1,m+1/2}, b\alpha^i_{2,m+1/2}\}; \qquad \tilde\alpha^i_{2,m+1/2} = \operatorname{minmod}\{\alpha^i_{2,m+1/2}, b\alpha^i_{1,m+1/2}\};$$

$$\tilde{\tilde\alpha}^i_{2,m+1/2} = \operatorname{minmod}\{\alpha^i_{2,m+1/2}, b\alpha^i_{3,m+1/2}\}; \qquad \tilde\alpha^i_{3,m+1/2} = \operatorname{minmod}\{\alpha^i_{3,m+1/2}, b\alpha^i_{2,m+1/2}\}.$$

In this equation, $b = (3-\varkappa)/(1-\varkappa)$, and the parameter $\varkappa$ determines schemes with different accuracy. The flux limiter has the form

$$\operatorname{minmod}(x, y) = \operatorname{sign}(x)\max\{0, \min[|x|, y\operatorname{sign}(x)]\}.$$

The step of integration in time is found from the estimates of inviscid and viscous fluxes

$$\frac{1}{\Delta t_i} = \frac{1}{\mathrm{CFL}}\max\Big\{\frac{1}{\Delta t^1_i}, \frac{\beta}{\Delta t^2_i}\Big\},$$

where CFL is the Courant–Friedrichs–Lewy number and $\beta \approx 0.5$. The time step Δt^1_i is calculated from the spectral radius of the Jacobian of the discrete inviscid operator, and the time step Δt^2_i is found from the quasi-linear form of viscous fluxes recorded in primitive variables and from the spectral radius of the Jacobian of the discrete inviscid operator [11].

The computational procedure is implemented as a sequence of the following steps.

1. Reconstruction of the solution in each control volume and extrapolation of unknowns to find the state of the flow on the control-volume faces from values prescribed in the center.

2. Solving the Riemann problem for each face of the control volume with allowance for the local flow direction (normal to the control-volume face).

3. Evolution of the time step.

The system of difference equations is solved by a multigrid method on the basis of a total approximation scheme (four grid levels and a V-cycle are used).

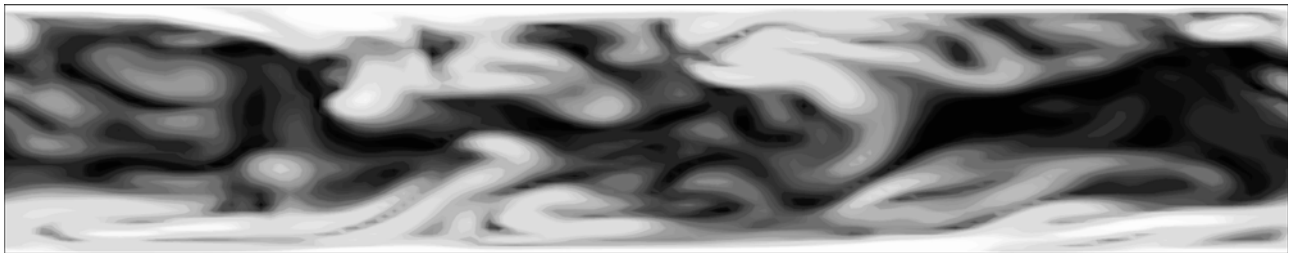

Fig. 1. Vortex flow pattern in a channel at $t = 0.32$ sec.

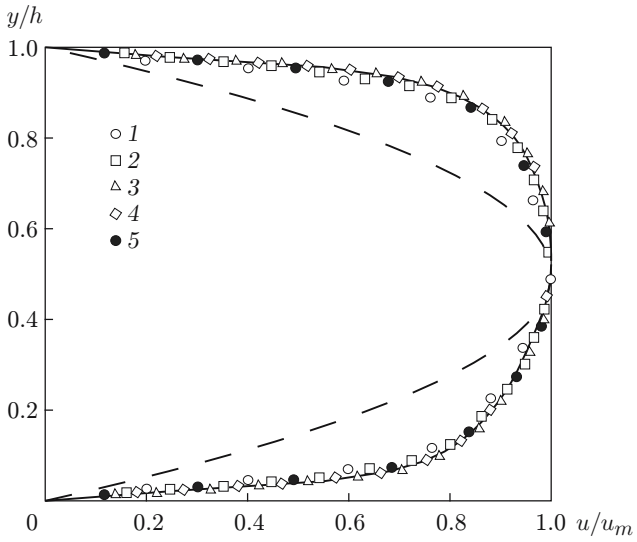

Fig. 2. Cross-sectional distribution of streamwise velocity: Smagorinsky model (1), Van Driest model (2), RNG version of the Smagorinsky model (3), dynamic model (solid curve), differential model of eddy viscosity (4), DNS data [2] (5), and laminar flow velocity profile (dashed curve).

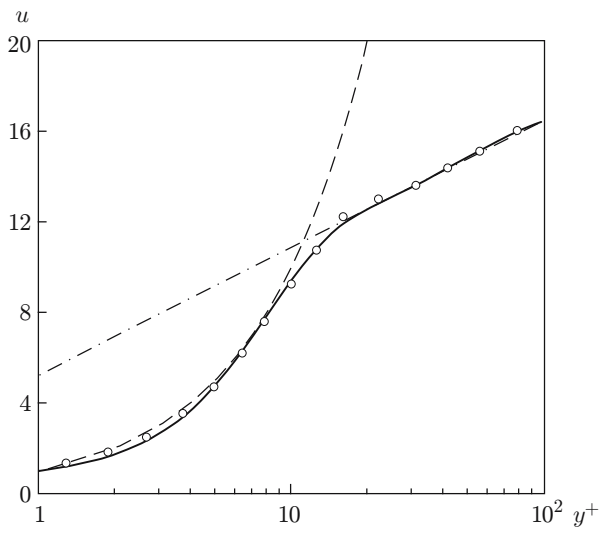

Fig. 3

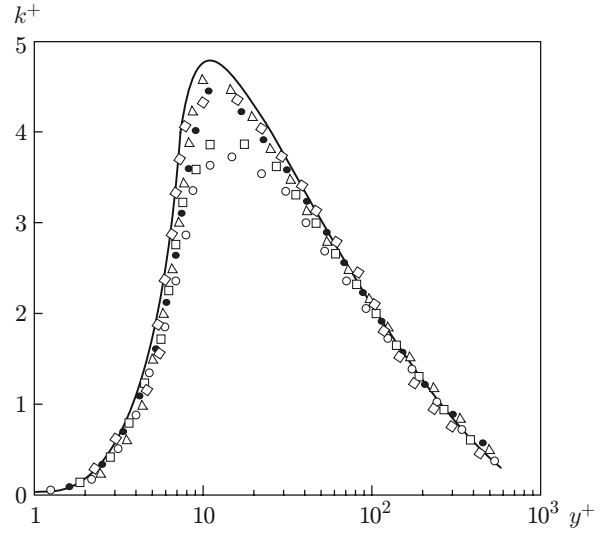

Fig. 4

Fig. 3. Velocity distribution in the boundary layer near the wall (solid curve): the points follow the Reichardt law [14]; the dashed and dot-and-dashed curves are the linear distribution of velocity in the viscous sublayer and the logarithmic distribution in the turbulent region of the boundary layer, respectively.

Fig. 4. Distribution of the turbulent kinetic energy in the vicinity of the wall: the filled points refer to the DNS data [2] for $\mathrm{Re}_\tau = 395$; the remaining point here and in Figs. 5–7 denote the same as those in Fig. 2.

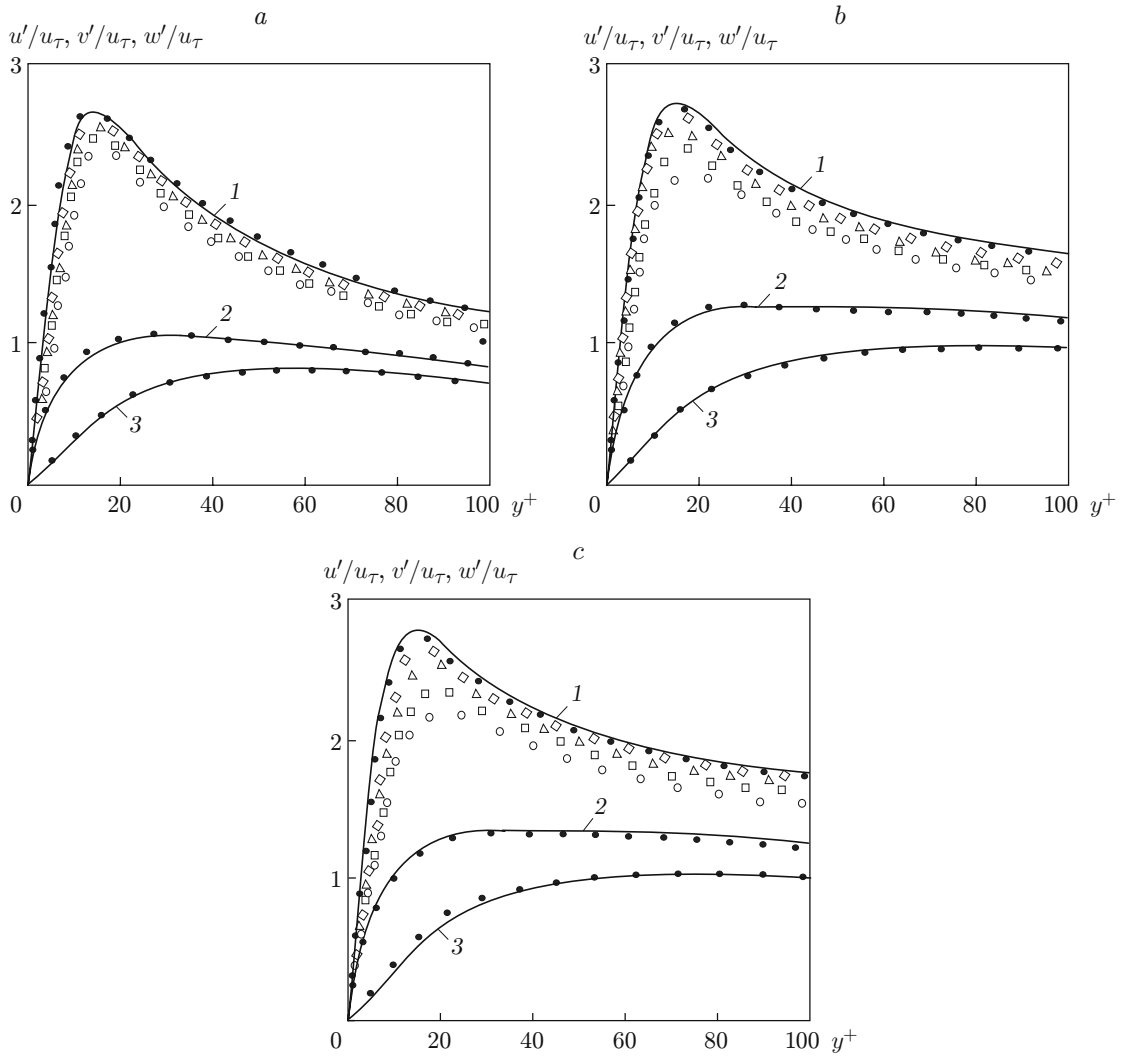

Fig. 5. Distributions of fluctuating components of velocity u' (1), v' (2), and w' (3) over the channel cross section for $\mathrm{Re}_\tau = 180$ (a), 360 (b), and 590 (c); the filled points refer to the data of [15, 16].

The use of LES also imposes some specific requirements to computational grids. As the value of effective viscosity is proportional to the grid step, an increase in the cell size in any direction can increase scheme viscosity and distort the results. That is why it is reasonable to use computational grids whose cells have approximately identical sizes in all coordinate directions, independent of the direction of gradients of the mean flow parameters.

6. Computation Results. The following values were assigned to flow parameters: $\rho_0 = 1.18$ kg/m^3, $u_0 = 180.0$ m/sec, $p_0 = 1.013 \cdot 10^5$ Pa, and $T_\mathrm{w} = 288$ K. The working medium had the following parameters: $\gamma = 1.4$, $R = 287.1$ J/(kg $\cdot$ K), $c_p = 1004.85$ J/(kg $\cdot$ K), $\mathrm{Pr} = 0.72$, and $\mathrm{Pr}_t = 0.80$. The characteristic parameter of the problem was assumed to be the Reynolds number $\mathrm{Re} = \rho_0 u_0 h/\mu_0$, which was varied within $\mathrm{Re} \approx 100$–6000 by appropriate changes in dynamic viscosity. The interval of the Reynolds number used corresponds to the range $\mathrm{Re}_\tau \approx 10$–$600$, where $\mathrm{Re}_\tau = \rho_0 u_\tau h/\mu_0$. The basic computational variant implied that $\mathrm{Re}_\tau = 360$ ($\mu = 0.039$ Pa $\cdot$ sec).

The computations were performed on a $150 \times 65 \times 65$ grid, being refined toward the walls and the entrance cross section of the channel. The maximum steps in the coordinate directions were $\Delta x = 0.052$ and $\Delta y = \Delta z = 0.045$. The time step was chosen to be $\Delta t = 0.00025$ sec. Forty thousand time steps were made to obtain a statistically reliable mean pattern of the flow. The chosen grid steps were approximately three times both Kolmogorov's length scale $l_k = (\nu^3/\varepsilon)^{1/4}$ and the scale ν/u_τ^2 constructed on the basis of dynamic viscosity.

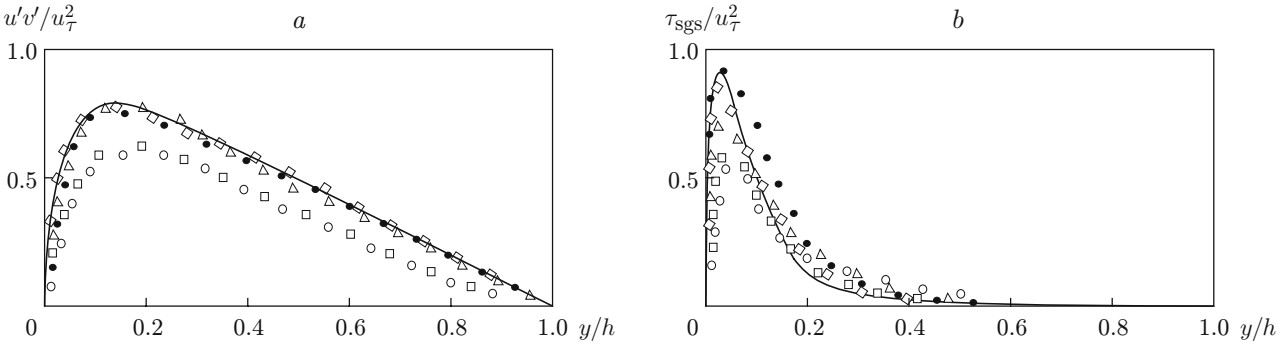

Fig. 6. Distributions of the turbulent Reynolds stresses (a) and subgrid turbulent stresses (b): the filled points refer to the results obtained by the Smagorinsky model.

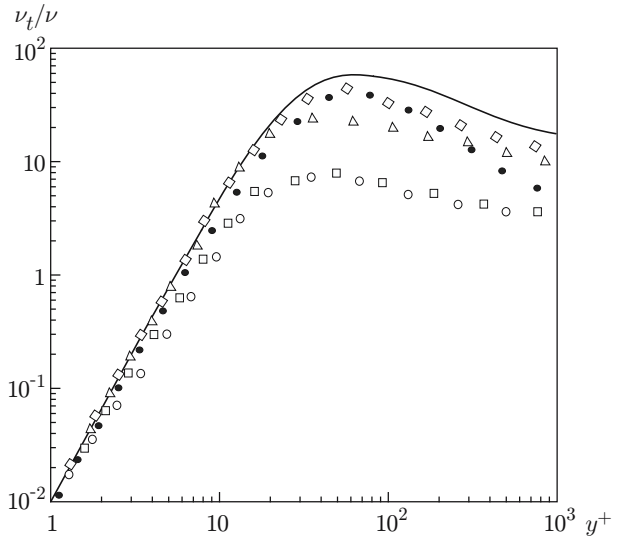

Fig. 7

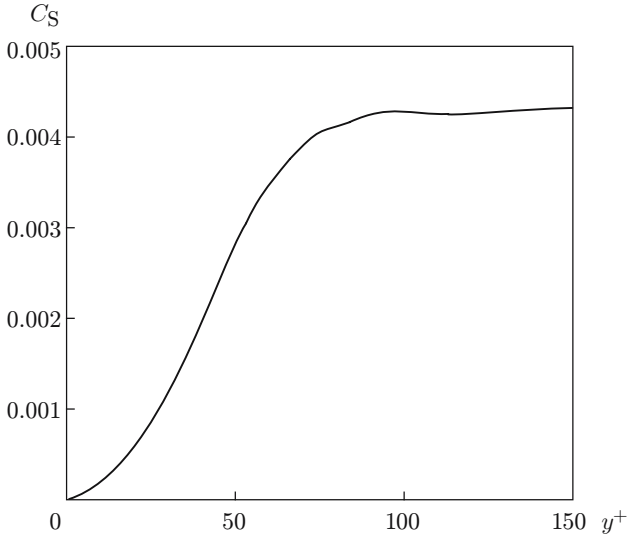

Fig. 8

Fig. 7. Distribution of turbulent viscosity near the wall: the filled points refer to the data of [16].

Fig. 8. Smagorinsky parameter versus the distance from the wall.

The instantaneous flow pattern in the channel was visualized by using the absolute value of velocity vorticity

$$\Omega = |\nabla \times \boldsymbol{v}| = (\Omega_x^2 + \Omega_y^2 + \Omega_z^2)^{1/2},$$

where Ω_x, Ω_y, and Ω_z are the vortex components in the coordinate directions x, y, and z, respectively. The channel-flow pattern presented in the form of lines with identical values of velocity vorticity is shown in Fig. 1.

The streamwise velocity profile in the channel cross section is shown in Fig. 2. The results obtained show that the Smagorinsky model yields a less filled profile of velocity than other models. Introduction of the Van Driest damping function improves the computed results, which become almost identical to those computed by the dynamic model.

The velocity distribution in the vicinity of the wall is in good agreement with the Reichardt law [14] constructed on the basis of experimental data and covering the viscous sublayer and the buffer and logarithmic regions of the boundary layer (Fig. 3). The results are in agreement with data computed by the dynamic model.

The computed turbulent kinetic energy is compared with its DNS values [2, 15] in Fig. 4. The distributions of fluctuating components of velocity in the channel cross section are plotted in Fig. 5 together with the data of [15, 16]. Though the Smagorinsky model and the Van Driest model underpredict the values of the fluctuating streamwise velocity component, the fluctuating velocity components v and w computed by different models are in fairly good

agreement with each other (the data presented refer to the dynamic model). The role of subgrid modeling becomes more important with increasing Reynolds number.

Figure 6 shows the distributions of turbulent Reynolds stresses and subgrid turbulent stresses. The turbulent viscosity ν_t in the boundary layer as a function of the distance from the wall is plotted in Fig. 7. The Smagorinsky model and the Van Driest model underpredict the values of turbulent viscosity. The best agreement with experimental data is provided by the dynamic and differential models.

The Smagorinsky parameter as a function of the distance from the channel wall, predicted by the dynamic model, is shown in Fig. 8.

The use of the RNG version of eddy viscosity and the dynamic and differential models increases the computational time by 18, 30, and 35%, respectively, as compared to the time spent on a computation without any subgrid model.

Conclusions. The accuracy and computational efficiency are compared for a number of models of subgrid eddy viscosity (Smagorinsky model, Van Dries model, RNG model, and dynamic and one-parameter models). By comparing the computed data with results of a physical experiment and direct numerical simulation, it is demonstrated that the use of the Smagorinsky model and the Van Driest model leads to rather large errors in predicting the fluctuating characteristics of the flow. At the same time, the models examined in the present paper offer fairly accurate estimates of the mean flow parameters.

The results obtained allow us to conclude that the role of subgrid modeling becomes more important with increasing Reynolds number.

REFERENCES

1. P. A. Libby and F. A. Williams (eds.), *Turbulent Reacting Flows*, Academic Press, New York (1994).
2. P. Moin and K. Mahesh, "Direct numerical simulation. A tool in turbulence research," *Annu. Rev. Fluid Mech.*, **30**, 539–578 (1998).
3. M. Strelets, "Detached eddy simulation of massively separated flows," AIAA Paper No. 2001-0879 (2001).
4. O. M. Belotserkovskii, *Numerical Simulation in Mechanics of Continuous Media* [in Russian], Fizmatlit, Moscow (1994).
5. C. Fureby, "On subgrid scale modeling in large eddy simulation of compressible fluid flow," *Phys. Fluids*, **8**, No. 5, 1301–1311 (1995).
6. U. Piomelli, "Large-eddy simulation: Achievements and challenges," *Prog. Aerospace Sci.*, **35**, 335–362 (1999).
7. P. R. Spalart, "Strategies for turbulence modelling and simulations," *Int. J. Heat Fluid Flow*, No. 21, 252–263 (2000).
8. J. Smagorinsky, "General circulation experiments with the primitive equations," *J. Basic Exp.*, **91**, 99–165 (1963).
9. K. Horiuti, "Backward scatter of subgrid-scale energy in wall-bounded and free shear turbulence," *J. Phys. Soc. Jpn.*, **66**, No. 1, 91–107 (1997).
10. M. Germano, U. Piomelli, P. Moin, and W. H. Cabot, "A dynamic subgrid scale eddy viscosity model," *Phys. Fluids*, **3**, No. 7, 1760–1765 (1991).
11. K. N. Volkov, "Application of the control-volume approach for solving problems of fluid dynamics on unstructured grids," *Vychisl. Met. Program.*, **6**, No. 1, 43–60 (2005).
12. S. Osher, "Riemann solvers, the entropy condition, and difference approximation," *SIAM J. Numer. Anal.*, **21**, No. 2, 217–235 (1984).
13. S. R. Chakravarthy and S. Osher, "A new class of high-accuracy TVD schemes for hyperbolic conservation laws," AIAA Paper No. 85-0363 (1985).
14. G. Schlichting, *Boundary Layer Theory*, McGraw-Hill, New York (1968).
15. R. D. Moser, J. Kim, and N. N. Mansour, "Direct numerical simulation of turbulent channel flow up to $\mathrm{Re}_\tau = 590$," *Phys. Fluids*, **11**, 943–945 (1999).
16. L. Temmerman, M. A. Leschziner, C. P. Mellen, and J. Frohlich, "Investigation of wall-function approximations and subgrid-scale models in large eddy simulation of separated flow in a channel with streamwise periodic constrictions," *Int. J. Heat Fluid Flow*, **24**, 157–180 (2003).